Science of the Total Environment – 2018

Influence of urban pattern on inundation flow in floodplains of lowland rivers

M. Bruwier[a], A. Mustafa[c], D.G. Aliaga [c], P. Archambeau[a], S. Erpicum[a], G. Nishida [c], X.W. Zhang [c], M. Pirotton[a], J. Teller[b] & B. Dewals[a]

[a] *Hydraulics in Environmental and Civil Engineering (HECE), University of Liege (ULG), Belgium*
[b] *Local Environment Management and Analysis (LEMA), University of Liege (ULG), Belgium*
[c] *Department of Computer Science, Purdue University, USA*

Corresponding author: mbruwier@ulg.ac.be, +3243669004

ABSTRACT:

The objective of this paper is to investigate the respective influence of various urban pattern characteristics on inundation flow. A set of 2,000 synthetic urban patterns were generated using an urban procedural model providing locations and shapes of streets and buildings over a square domain of 1 x 1 km². Steady two-dimensional hydraulic computations were performed over the 2,000 urban patterns with identical hydraulic boundary conditions. To run such a large amount of simulations, the computational efficiency of the hydraulic model was improved by using an anisotropic porosity model. This model computes on relatively coarse computational cells, but preserves information from the detailed topographic data through porosity parameters. Relationships between urban characteristics and the computed inundation water depths have been based on multiple linear regressions. Finally, a simple mechanistic model based on two district-scale porosity parameters, combining several urban characteristics, is shown to capture satisfactorily the influence of urban characteristics on inundation water depths. The findings of this study give guidelines for more flood-resilient urban planning.

Keywords: Urban floods, flood mitigation, porosity hydraulic model, procedural modelling.

1. INTRODUCTION

In literature, most existing studies analyse many aspects of the influence of urbanization on floods but generally disregard the impact of the urban pattern geometry on the severity of flooding. However, the urban characteristics (e.g. street width, orientation or curvature) may have a strong influence on inundation flow since they influence the discharge partition between the streets as well as the flow depths and velocities.

Vollmer et al. (2015) and Lin et al. (2016) investigated the interactions between urbanization and inundation flow for the rehabilitation of Ciliwung River in Jakarta, Indonesia. The inundation extent and water depths were compared between different rehabilitation scenarios to identify the most effective one to mitigate floods. Since these authors considered rehabilitation scenarios specific to their case study, their conclusions are difficult to generalize to other urban areas. Huang et al. (2014) studied the impact of building coverage on the increase of water depths for a rectangular flume with an array of aligned buildings obstructing the flow. They proposed a method to update the Manning roughness coefficient according to the blockage effect of buildings but consider only one urban characteristic (i.e., building coverage) of an idealized urban network.

In this paper, we present a more systematic analysis to determine the respective influence of various urban planning characteristics on inundation water depths. We followed a three-step procedure. First, we used an urban procedural model to generate 2,000 quasi-realistic building layouts by varying randomly the values of 10 urban model parameters: average street length, street orientation, street curvature, major and minor street widths, parks coverage, mean parcel area and building setbacks (i.e. recess of a building from the parcel borders).

Second, we computed the inundation flow field for each building layout by considering the same hydraulic boundary conditions. To make the hydraulic computation tractable for the 2,000 synthetic urban configurations, we used subgrid models which enable a reduction of the

computational cost thanks to a coarsening of the computational grid while preserving the essence of the detailed topographic information. We opted for an anisotropic porosity model, in which fine scale topographic information are preserved at the coarse scale by means of porosity parameters involved in the governing equations (Sanders et al. 2008).

Finally, the influence of nine urban characteristics on the computed water depths were analysed based on multiple linear regressions (MLR) and on Pearson correlation coefficients. Additionally, a conceptual model was developed to investigate the relationships between the inundation water depths and district-scale storage and conveyance porosity parameters, evaluated as a combination of the urban characteristics. The results show a good predictive capacity of the model based on just the two porosity parameters, with a prevailing influence of district-scale conveyance porosity. Hence, this model enables quantifying to which extent flood-related impacts of an increase in the building coverage (i.e. new developments) can be mitigated by an appropriately chosen layout of the buildings.

In the present analysis, we decided to keep the terrain slope equal to zero and to consider just one steady flooding scenario so as to focus on the influence of the urban planning characteristics. Therefore, the conclusions do not apply for floodplains involving steep slopes; but are instead representative of floodplains of lowland rivers which are flooded gradually and with moderate flow velocity. The steady flow conditions considered here are a valid representation of long duration floods (e.g., in lowland rivers such as the Rhine or the Meuse); but not for short duration floods in steep rivers nor for flash flood events.

In section 2, we introduce the procedural modelling used to generate the synthetic building layouts, and we briefly describe the hydraulic model used to compute the flow characteristics in the urban area. We also present the statistical approach followed to process the modelling results. The results are presented in section 3, in terms of generated building layouts, computed flow fields and influence of urban characteristics on the flood severity upstream of the urban area.

Finally, we provide an in-depth discussion of the results (section 4), by testing their sensitivity with respect to the number and choice of input variables, the sample size and the model selection, as well as by developing a conceptual model (based on district-scale porosity parameters) which agrees remarkably well with the results of the detailed numerical simulations.

2. METHOD

As sketched in the flowchart of Figure 1, we set up a three-step methodology to analyse the influence of the building layout on inundation flow:

- first, procedural modelling was used to generate about 2,000 synthetic urban layouts considering ten input parameters, including typical street length, width and curvature, mean parcel area, setbacks … (section 2.1);
- second, by means of a porosity-based hydraulic model, the flow characteristics were computed for each urban layout, considering identical hydraulic boundary conditions (section 2.2);
- finally, based on Pearson correlation coefficients and on multiple linear regression, we highlight the sensitivity of inundation flow to the input parameters (section 2.3).

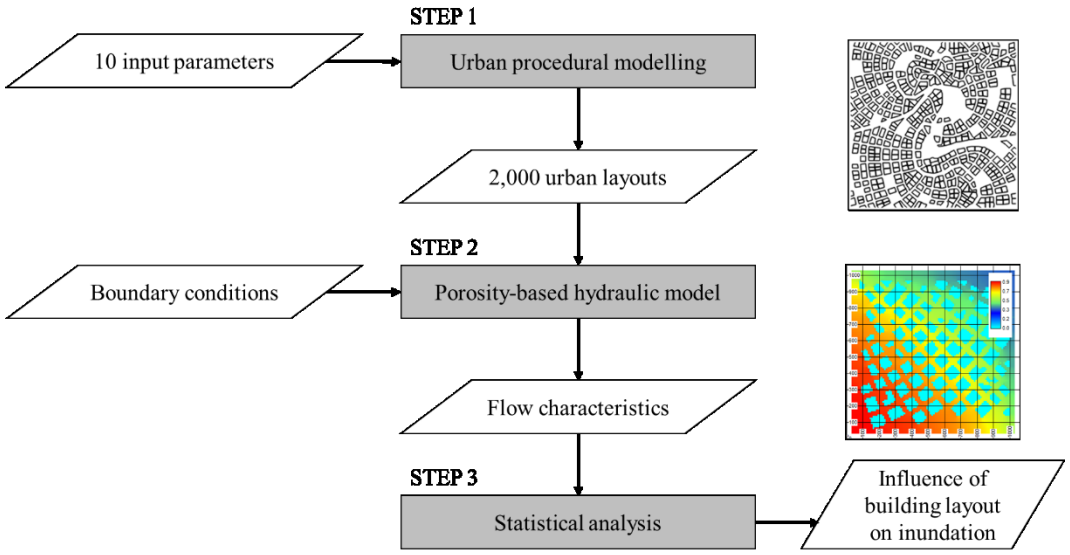

Figure 1 : Methodology for the determination of the influence of building layout on inundation characteristics.

2.1. Procedural modelling of urban layouts

Procedural modelling of urban layouts consists in automatically generating urban layouts based on a set of rules and parameter values (Prusinkiewicz and Lindenmayer 1990). The output of procedural modelling is a collection of locations and shapes of streets and buildings.

Here, we used an upgraded version of the method originally proposed by Parish and Müller (2001), as described in Vanegas et al. (2009) to support more variations in the street networks. The procedural modelling technique used is deterministic, in the sense that, for a given set of values of the input parameters, it generates a single urban layout.

We considered ten input parameters, which are all of practical relevance for urban planning. They include street characteristics (typical length, orientation, curvature and width), park coverage, mean parcel area and setbacks (Table 1).

As sketched in Figure 2, the procedural modelling involves mainly three steps:

- generation of a "skeleton" of the network of streets (i.e. the street centrelines), based on the typical street length L_s, orientation α and curvature χ (Figure 2a);

- calculation of parcels based on the widths W and w of major and minor streets, the park coverage P_c and the mean parcel area A_p (Figure 2b);
- creation of the building footprints based on values for the front setback s_f (recess of a building from the street, as shown in Figure 2c), rear setback s_r (recess of a building from the parcel border on the backyard side) and side setback s_s (recess of a building from the lateral parcel borders, which relates to building separation).

To ensure the representativity of real-world urban configurations, plausible ranges of variation of the input parameters were determined from cadastral data of urban areas in the Walloon region, Belgium (Table 1). By selecting randomly parameter values in their respective ranges of variation, we generated 2,000 urban layouts, covering each a square area of 1 km by 1 km. In Table 1, the minimum value of the side setback is 1 m. Therefore, configurations with a free space enclosed within a building ($s_s = 0$) are not considered. However, the findings the study can be extended to these specific urban patterns by increasing the building coverage to reproduce the lack of access of the flow to the enclosed free-spaces.

	Urban parameter	Minimum	Maximum
L_s	Average street length	40 m	400 m
α	Street orientation	0°	180°
χ	Street curvature	0 km^{-1}	10 km^{-1}.
W	Major street width	16 m	33 m
w	Minor street width	8 m	16 m
P_c	Park coverage	5%	40%
A_p	Mean parcel area	350 m^2	1,100 m^2
s_f	Building front setback	1 m	5 m
s_r	Building rear setback	1 m	5 m
s_s	Building side setback	1 m	5 m

Table 1: Input urban parameters for the urban procedural modelling.

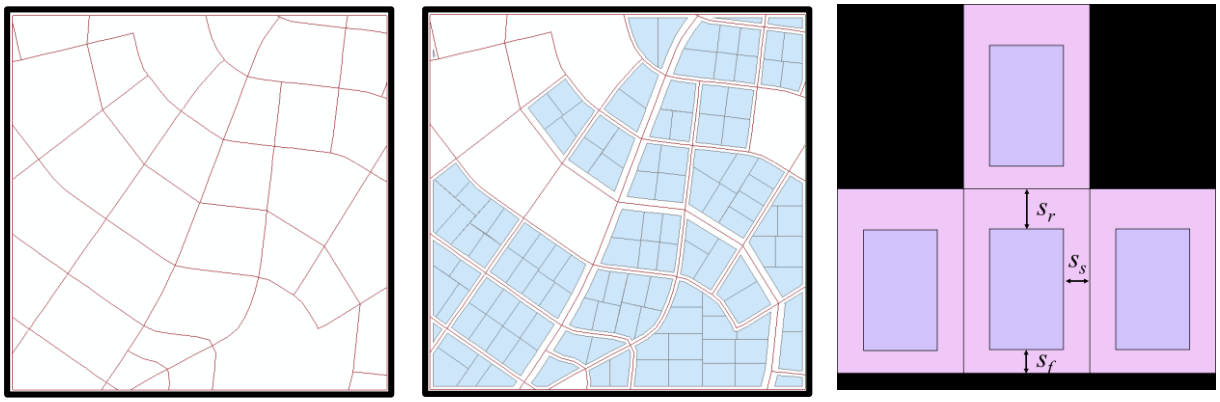

(a) Definition of the tensor field of the streets.

(b) Definition of the parcels and park areas.

(c) Definition of building footprint in each parcel.

Figure 2 : Main steps of procedural modelling of urban layouts.

Only the building footprints have an influence on the performed hydraulic computations. This enables merging some of the parameters listed in Table 1. For instance, parameters W (or w) and s_f should not be considered independently. Indeed, urban layouts characterized by distinct values

of the street width W (or w) and front setback s_f, but with the same value of the sum $W + 2\ s_f$ (or $w + 2\ s_f$) would lead to the same distance between the buildings located on either sides of a street. This distance should be retained as the parameter which actually controls the flow conveyance through this street, instead of W (or w) and s_f independently. Therefore, although the parameters listed in Table 1 are the real inputs of the procedural modelling, we performed the statistical analysis of the results by considering a slightly modified set of variables (Table 2):

- Parameters W, w and s_f were replaced by just two variables: $x_4 = W + 2\ s_f$ and $x_5 = w + 2\ s_f$.
- To account for the periodicity in the street orientation resulting from the symmetry of the domain and boundary conditions, the orientation parameter α was replaced by variable $x_2 = \left|\sin\left(2\left(\alpha - 45°\right)\right)\right|$ (Figure 3).
- The park coverage P_c was not kept alone; but lumped into an overall *building coverage* ratio x_9, evaluated as the ratio between the total area of building footprints and the area of the whole district (1 km^2). Variable x_9 is a function of all input parameters.
- All other variables were each kept equal to one of the remaining input parameters listed in Table 1.

Variable definition	Minimum	Maximum
$x_1 = L_s$	40 m	400 m
$x_2 = \left\|\sin\left(2\left(\alpha - 45°\right)\right)\right\|$	0	1
$x_3 = \chi$	0 km^{-1}	10 km^{-1}
$x_4 = W + 2\ s_f$	18 m	38 m
$x_5 = w + 2\ s_f$	10 m	21 m
$x_6 = A_p$	350 m^2	1,100 m^2
$x_7 = s_r$	1 m	5 m
$x_8 = s_s$	1 m	5 m
$x_9 = f(L_s, \alpha, \chi, W, w, P_c, A_p, s_r, s_f, s_s)$	0%	43%

Table 2: Variables used for the statistical analysis of the modelling results.

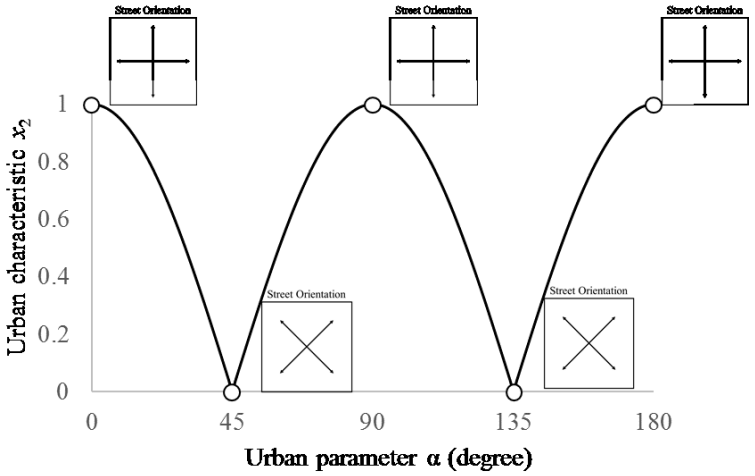

Figure 3 : Relation between variable x_2 and street orientation parameter α.

2.2. Porosity-based hydraulic modelling

In a second step, we applied an efficient hydraulic model to compute the flow characteristics for each of the 2,000 building layouts, under the same hydraulic boundary conditions. The terrain

was assumed horizontal and infiltration in the soil was neglected because it has a limited influence on river flooding in urbanized floodplains.

2.2.1. Model description

Two-dimensional shallow-water hydraulic models are considered state-of-the-art for the simulation of inundation flow in urban areas (El Kadi Abderrezzak et al. 2009, Ghostine et al. 2015). In such model, the buildings are idealized as impervious obstacles sufficiently high for not being overtopped by the flood. In general, three approaches can be considered to account for obstacles in inundation modelling (Schubert and Sanders 2012, Dottori et al. 2013): (*i*) increasing the roughness parameter, (*ii*) representing the obstacles as holes in the mesh or (*iii*) using a porosity-based model. The first one is particularly crude and requires calibration on a case-by-case basis. In the second one, each building needs to be explicitly resolved in the computational mesh, which makes this approach not suitable to investigate efficiently the 2,000 building layouts. In contrast, Schubert and Sanders (2012) showed that porosity-based models lead to the best balance between accuracy and run-time efficiency. They enable a coarsening of the mesh size by roughly one order of magnitude while preserving a good level of accuracy (Schubert and Sanders 2012, Kim et al. 2014, 2015, Özgen et al. 2016b, Bruwier et al. 2017a). Therefore, we opted here for this third option.

The shallow-water model with porosity used here was described in section 5.2 of Arrault et al. (2016) as well as in Bruwier et al. (2017a) and a comprehensive validation is presented in Bruwier et al. (2017b). It involves two types of porosity parameters: a storage porosity, defined at the centre of each cell, represents the void fraction in the cell while anisotropic conveyance porosities, defined at the edges of the computational cells, reproduce the blockage effect due to obstacles (Sanders et al. 2008, Chen et al. 2012, Özgen et al. 2016a). The values of these porosity parameters were determined geometrically from the building footprints.

The momentum equations involve the same drag loss term as in the formulation of Schubert and Sanders (2012). The drag coefficient c_D was set to the standard value $c_D = 3.0$. Bottom friction is modelled by Manning formula with a uniform roughness coefficient $n = 0.04$ sm$^{-1/3}$. This value of the roughness coefficient is comparable with the values suggested by Bazin (2013) and Mignot et al. (2006) to account for the various sources of flow resistances in urban areas such as bottom friction and small scale obstacles (debris, cars, urban furniture, etc.).

The numerical discretization is based on a conservative finite volume scheme and a self-developed flux-vector splitting (Erpicum et al. 2010). We used a Cartesian grid with a grid spacing of 10 m, which is comparable to the typical size of the buildings (> 15 m) but the porosity parameters enable the fine-scale geometric features to be accounted for.

To enhance computational efficiency in the presence of low values of the storage porosity ϕ, we used a merging technique which consists in merging each cell having a low value of storage porosity ($\phi < \phi_{min} = 10\%$) with a neighbouring cell (Bruwier et al. 2017a).

As detailed in Arrault et al. (2016) and Bruwier et al. (2017a, b), the model was successfully validated against fine scale computations and against experimental data for flow conditions similar to those prevailing here. The model is part of the academic code Wolf2D which was used in multiple flood risk studies (Ernst et al. 2010, Beckers et al. 2013, Bruwier et al. 2015).

2.2.2. Boundary conditions

The west and south sides of the computational domain are the upstream boundaries, while the east and north sides are the downstream ones. Along the upstream sides of the computational domain, a 30-m wide strip was kept free of buildings.

A total steady inflow discharge of 200 m^3/s, uniformly distributed, was prescribed as boundary condition along the upstream sides (unit discharge of 0.1 m^2/s). Along the downstream sides, the

outflow discharge q_j in each cell j was prescribed as a function of the computed water depth h_j in the cell by using a rating curve:

$$q_j = C_1 \Delta x \sqrt{2g\left(h_j - C_2\right)^3} \quad (1)$$

with Δx the grid spacing, g the gravity acceleration and constants C_1 and C_2 respectively equal to 0.5 and 0.3.

These boundary conditions are somehow arbitrary; but they lead to flow conditions in the network of streets which are representative of typical flooding in floodplains of lowland rivers. The duration of flood waves in such rivers may be as long as two to three weeks (e.g., de Wit et al. 2007), which enables describing the inundation flow in the floodplains as quasi-steady, consistently with the approach adopted here. Also, the downstream boundary conditions expressed by Eq. (1) leads to Froude numbers in our simulation domain ranging between 0.1 and 0.4, which matches detailed flow computations performed for typical real-world floodplains of lowland rivers (Beckers et al. 2013, Detrembleur et al. 2015).

2.3. Statistical analysis

The outcome of steps 1 and 2 of the methodology (Figure 1) consists in a set of 2,000 gridded flow characteristics data, representing the water depth and the two components of horizontal flow velocity in the 10,000 cells of the computational mesh. To make the subsequent analyses tractable, we synthetized the dataset by means of a single indicator y of flood severity for each of the 2,000 building layouts. We focused on the increase of the 90th percentile of the computed water depths along the upstream boundary of the domain (noted Δh_{90}) compared to a configuration without any buildings (h_{90} = 61 cm). This quantity is representative of the overall flow resistance (or loss of flow conveyance) induced by the layout of buildings and, hence, of the increase in flood levels that the presence of the buildings causes upstream of the considered area.

If the buildings result from new development, indicator $y = \Delta h_{90}$ reflects the impact of this development on flood danger upstream.

We performed the statistical analysis of the results by considering standardized variables, noted $\bar{x}_i$ (i = 1 to 9) and $\bar{y}$, defined as:

$$\bar{x}_i = \frac{x_i - x_{i,\text{mean}}}{x_{i,\text{std}}} \quad \text{and} \quad \bar{y} = \frac{y - y_{\text{mean}}}{y_{\text{std}}} \tag{2}$$

with $x_{i,\text{mean}}$ and $x_{i,\text{std}}$ (resp. y_{mean} and y_{std}) the mean and standard deviation of the variable x_i (resp. y) over all the building layouts.

We introduce the matrix notations **X** and **Y** with $\bar{x}_i^N$ and $\bar{y}^n$ the values of $\bar{x}_i$ and $\bar{y}$ corresponding to the n^{th} building layout:

$$\mathbf{X} = \begin{bmatrix} \bar{x}_1^1 & \bar{x}_2^1 & \cdots \\ \bar{x}_1^2 & \bar{x}_2^2 & \cdots \\ \vdots & \vdots & \ddots \\ \bar{x}_1^N & \bar{x}_2^N & \cdots \end{bmatrix} \quad \vdots \quad \text{and} \quad \mathbf{Y} = \begin{bmatrix} \bar{y}^1 \\ \bar{y}^2 \\ \vdots \\ \bar{y}^N \end{bmatrix} \tag{3}$$

with N being the number of building layouts.

The influence of each of the nine variables x_i on the inundation indicator y was determined using a multiple linear regression (MLR). The outputs of the regression are the least square linear coefficients $\mathbf{A} = [a_1, a_2, ..., a_9]^T$, computed from Eq. (4) and representing the sensitivity of y with respect to each variable x_i:

$$\mathbf{A} = \left(\mathbf{X}^{\mathrm{T}}\mathbf{X}\right)^{-1}\mathbf{X}^{\mathrm{T}}\mathbf{Y}. \tag{4}$$

We also used Pearson correlation coefficients ρ_i (section 4.1.4), defined as:

$$\rho_i = \frac{\mathrm{cov}(x_i, y)}{x_{i,\mathrm{std}}\ y_{\mathrm{std}}} = \frac{1}{N-1}\sum_{k=1}^{N}\left(\frac{x_i^k - x_{i,\mathrm{mean}}}{x_{i,\mathrm{std}}}\right)\left(\frac{y^k - y_{\mathrm{mean}}}{y_{\mathrm{std}}}\right) = \frac{1}{N-1}\sum_{k=1}^{N}\overline{x}_i^k\,\overline{y}^k \ . \qquad (5)$$

3. RESULTS

In this section, we first describe examples of synthetic building layouts obtained by procedural modelling (section 3.1). Next, we discuss the results of the hydraulic simulations (section 3.2) and, finally, we detail the outcomes of the statistical analysis of the simulation results (section 3.3).

3.1. Urban layouts

Figure 4 displays six of the 2,000 generated building layouts to enable the reader to appreciate the influence of the main input parameters (Table 1 and Table 2). The variables x_1 to x_9 corresponding to the six building layouts of Figure 4 are given in Table 3.

Layout (a) and (b) in Figure 4 correspond to the same input parameters, except for the average street length x_1 and street curvature x_3. In layout (a), the average street length is about 3.4 times higher than in layout (b). This results in a more "fragmented" urban pattern in layout (b) compared to layout (a). Indeed, apart from the change in street curvature, layout (a) shows substantially larger building blocks than in layout (b). This observation also applies when layouts (c) and (d) are compared, as the average street length x_1 in layout (c) is almost three times higher than in layout (d). Layout (d) exemplifies an urban pattern characterized by a high value of the street curvature x_3. Comparing the building layouts (c) and (d) also reveals that the mean parcel area x_6 has a significant influence on the size of the building footprints, as x_6 takes a value roughly three times larger in the case of layout (c) than for layout (d).

The street orientation (x_2) has a strong influence on the connectivity between the different faces. For instance, in layout (a) ($x_2 = 0$) the building alignment tends to guide the flow entering through the west (resp. south) upstream face towards the north (resp. east) downstream face. In contrast,

layout (f) ($x_2 \approx 1$) seems to promote flow connection from the west (resp. south) upstream face towards the east (resp. north) downstream face.

The building rear setback x_7 is of little significance in our analysis as it mainly controls the distance between the back of the buildings and the limit of the corresponding plot of land. This distance has no direct influence on the flow computation. In contrast, the side setback x_8 plays a major part since it controls the distance in-between adjacent buildings and hence the possibility for water to penetrate inside a block of buildings. This is exemplified by building layouts (e) and (f). The side setback x_8 in the former layout is twice smaller than in the latter.

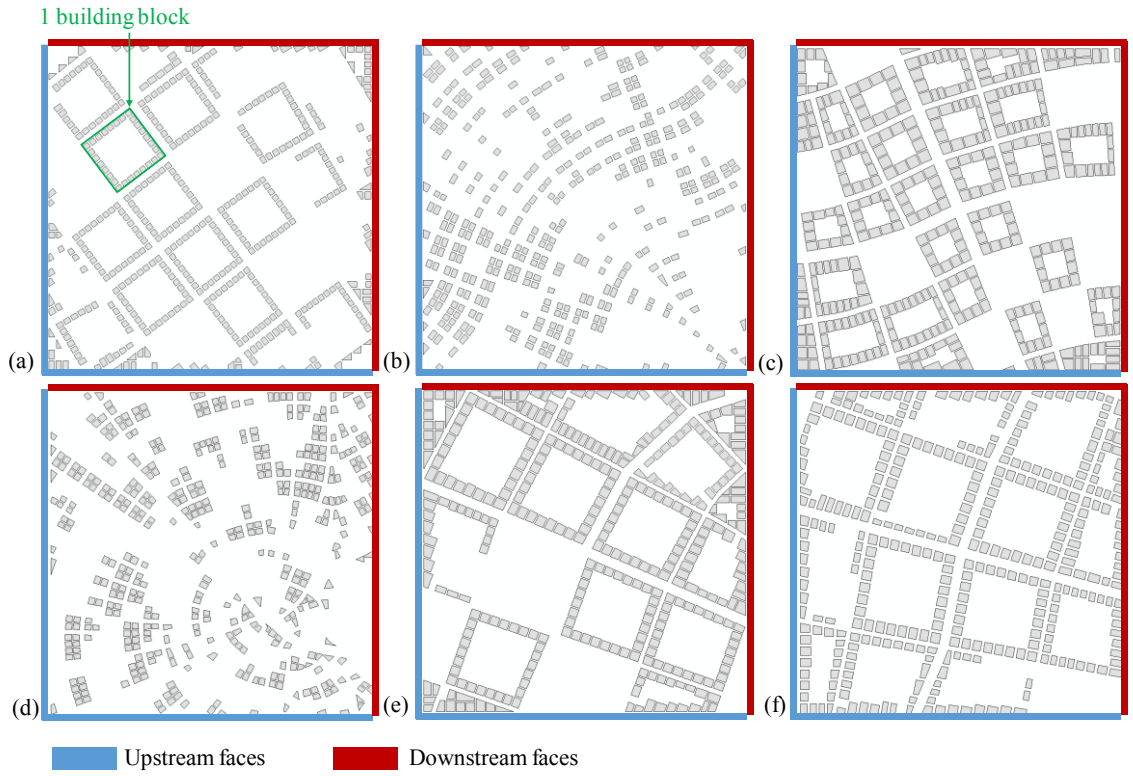

Figure 4: Building footprints for six out of the 2,000 layouts generated by procedural modelling.

Conf.	x_1	x_2	x_3	x_4	x_5	x_6	x_7	x_8	x_9	h_{90}
a)	199 m	0	0.5 km^{-1}	28 m	18 m	500 m^2	3.0 m	3.0 m	13%	0.79 m
b)	59 m	0	1.7 km^{-1}	28 m	18 m	500 m^2	3.0 m	3.0 m	13%	0.74 m
c)	165 m	0.58	0.7 km^{-1}	35 m	15 m	1066 m^2	2.2 m	2.1 m	33%	1.02m
d)	57 m	0.15	3.9 km^{-1}	29 m	12 m	370 m^2	1.4 m	2.0 m	15%	0.75 m
e)	274 m	0.97	1.4 km^{-1}	28 m	11 m	880 m^2	2.5 m	2.3 m	26%	1.00 m
f)	293 m	0.97	0.5 km^{-1}	28 m	11 m	872 m^2	2.3 m	4.6 m	22%	0.86 m

Table 3: Variables x_1 to x_9 characterizing the six building layouts displayed in Figure 4.

3.2. Hydraulic simulations

3.2.1. Calibration / validation of the porosity-based model

The coarse model errors on the water depths are expected to be lower than 5% without any drag loss term while a reduction up to only 0.5% error can be obtained with an optimal calibration of the drag coefficient (Bruwier et al. 2017a). Based on very different building layouts, it was shown that the range of variation of the optimal drag coefficient falls between 2.0 and 3.0 for the urban configurations considered in this study. Therefore, using a constant drag coefficient $c_{D,0}^{b} = 3.0$ for all computations, the coarse model error on the water depths should not exceed a few percent.

3.2.2. Computed water depths and velocity fields

The results of the hydraulic simulations are 2D maps of computed water depths and velocity fields. Figure 5 shows examples of hydraulic modelling results for the building layouts (c), (d) and (f) defined in Figure 4. The white areas in the maps of Figure 5 correspond to holes in the computational domain, i.e. cells which are inactive because they are mostly included within a building and therefore excluded from the computation. For layouts (c) and (f), virtually all buildings are reproduced explicitly by holes in the computational domain and the porosity parameters enable improving the geometric description of inclined boundaries. In contrast, much of the urban pattern of layout (d) is reflected only through the porosity parameters because in this case the buildings have a typical size comparable to the grid spacing. This results from the relatively low value of the mean parcel area x_6 in layout (d) (Table 3).

The computed water depths are minimum close to the downstream faces (north and east) and maximum along the upstream faces (west and south), due to the overall flow resistance induced by the buildings. The selected flood level indicator h_{90} along the upstream faces varies between

0.61 m and 1.14 m. Hence, for the tested configurations, varying the building layout may change the upstream flood level by a factor of almost two.

Overall the flow remains relatively slow within the urban area, with a Froude number $F = ||\boldsymbol{v}|| / (g\, h)^{0.5}$ of the order of 0.1 ($||\boldsymbol{v}||$ represents the velocity magnitude). The maximum value of F does not exceed about 0.4. The velocity increases at local contractions. This is particularly visible in layout (f), which is characterized by a side setback x_8 more than twice larger than for layouts (c) and (d), enabling hence more intense flow exchanges between the streets and the void areas inside building blocks ("courtyards"). This is also remarkably shown by the higher flow velocity computed inside the building block in layout (f) (velocity magnitude ~ 0.20 m/s) compared to layout (c) (velocity magnitude ~ 0.1 m/s). This results also from the higher side setback value (x_8) in the former layout compared to the latter (Figure 4), making the void area within the building blocks more accessible to the flow in layout (f). The absolute velocities are high around the top-left and bottom-right corners where the flow avoids passing through the building area.

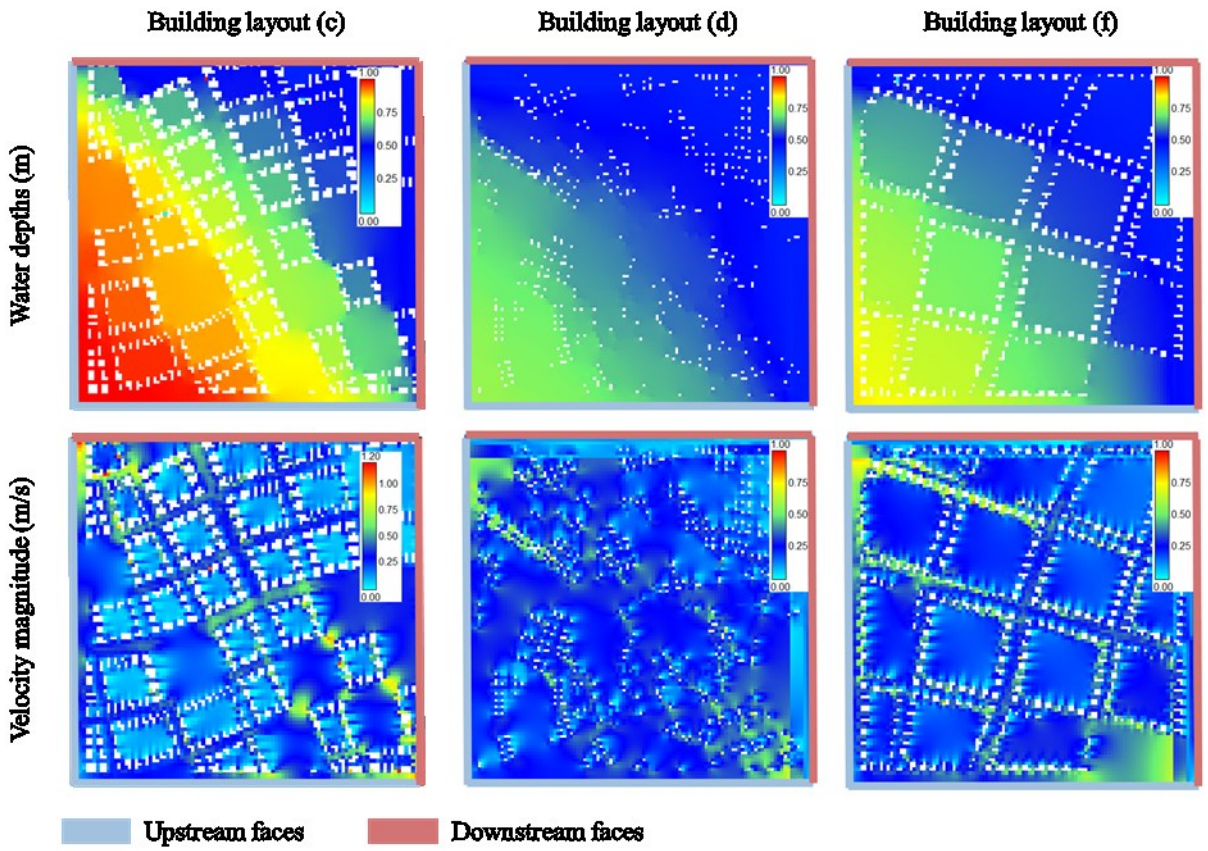

Figure 5: Representation of water depths and flow fields for some urban patterns.

3.3. Influence of urban characteristics on inundation water depths

Figure 6 shows the regression coefficients a_i computed with Eq. (4) for an inundation indicator $y = \Delta h_{90}$ computed based on the 90th percentile of the computed water depths along the upstream boundaries of the domain (section 2.3). A positive value for a regression coefficient a_i indicates that an increase in the corresponding variable x_i leads to an increase in the water depths, and conversely for a negative value of the regression coefficient. Using the regression coefficients of Figure 6, the Δh_{90} values can be predicted with a mean absolute error and a root mean square error of, respectively, 2.3 cm and 2.9 cm. This represents less than 15% of the mean value of Δh_{90} (21.3 cm).

The results of the multiple linear regression (MLR) show that the building coverage (x_9) is by far the most influential urban characteristics. Besides the building coverage, the average street length (x_1) has also a substantial influence on the water depths, because it controls the size of the building

blocks. As shown in section 3.1, the lower the value of the average street length is, the more "fragmented" the urban patterns are. This contributes to avoid the creation of void areas surrounded by buildings, which are therefore not easily accessible to the flow. In a more fragmented urban pattern, a larger portion of void area contributes to the flow conveyance. Similarly, reducing of the building side setback (x_8) leads to higher water depths (section 3.2), due to the reduction of the conveyance capacity between adjacent buildings. This is consistent with the negative value obtained for coefficient a_8.

The increase in building size resulting from an increase in the mean parcel area (x_6) leads to higher water depths, as reflected by the positive value of a_6. The street orientation (x_2) and curvature (x_3) seem to have no significant influence on the water depths. This is certainly a result of the relatively low values of flow velocity in the considered urban area ($F \sim 0.1$), which are typical of lowland rivers. This finding is expected not to apply in the case of floodplains characterized by steeper topographic gradients, where the flow velocity would be higher and more dynamic effects would prevail.

The insignificant influence of the rear setback (x_7) can be explained by the weak influence of this variable on the flow conveyance since it mainly describes the void area within building blocks, which contribute anyway only very little to the overall flow conveyance through the urban area.

While the results of the MLR show no influence of the major street width (x_4) on the inundation water depths, a slight influence is shown for the minor street width (x_5). This should be explained by the high number of minor streets in the urban domain compared to only two major streets.

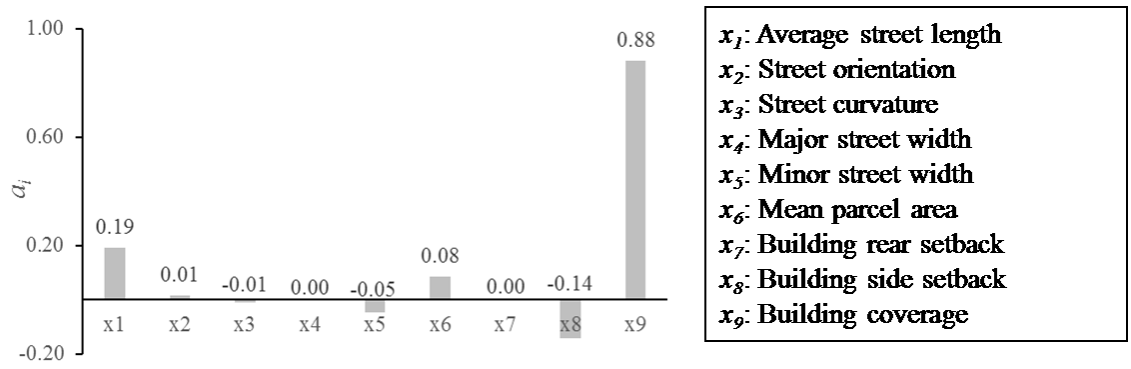

Figure 6: Regression coefficients a_i of the urban characteristics for Δh_{90}.

4. DISCUSSION

The results are discussed here, based on a comprehensive sensitivity analysis (section 4.1) and by comparing them with those of a simple conceptual approach (section 4.2).

4.1. Sensitivity analysis

4.1.1. Indicator of inundation water depths

The performed analysis is based on the increase of the 90th percentile of the water depths computed along the upstream boundaries of the urban area: Δh_{90}. Here, we test to which extent the conclusions of the analysis remain valid when another indicator of flood severity is chosen instead of Δh_{90}. To do so, we repeated the analysis by considering percentiles from 50th to 90th with a constant step of 5th and these percentiles were evaluated either along the upstream boundaries of the domain, or throughout the whole domain.

In Figure 7a, the sensitivity of the results of the MLR to the selection of the indicator of flood severity is shown through boxplots representing the variation of each coefficient a_i when all options described in 3.3 are tested. This sensitivity remains low for all coefficients a_i. Coefficients a_1 and a_6 corresponding to the influence of the average street length (x_1) and the mean parcel area (x_6) show the highest sensitivity with values ranging respectively from 1.3×10^{-1} to 2.1×10^{-1} and from 1.0×10^{-2} to 8.3×10^{-2}. Nonetheless, the findings described in section 3.3 remain

generally valid whatever the choice of the indicator of flood severity. Comparing Figure 7b and Figure 7c, the sensitivity of the results to the percentiles is higher when they are evaluated throughout the whole domain than along the upstream boundary.

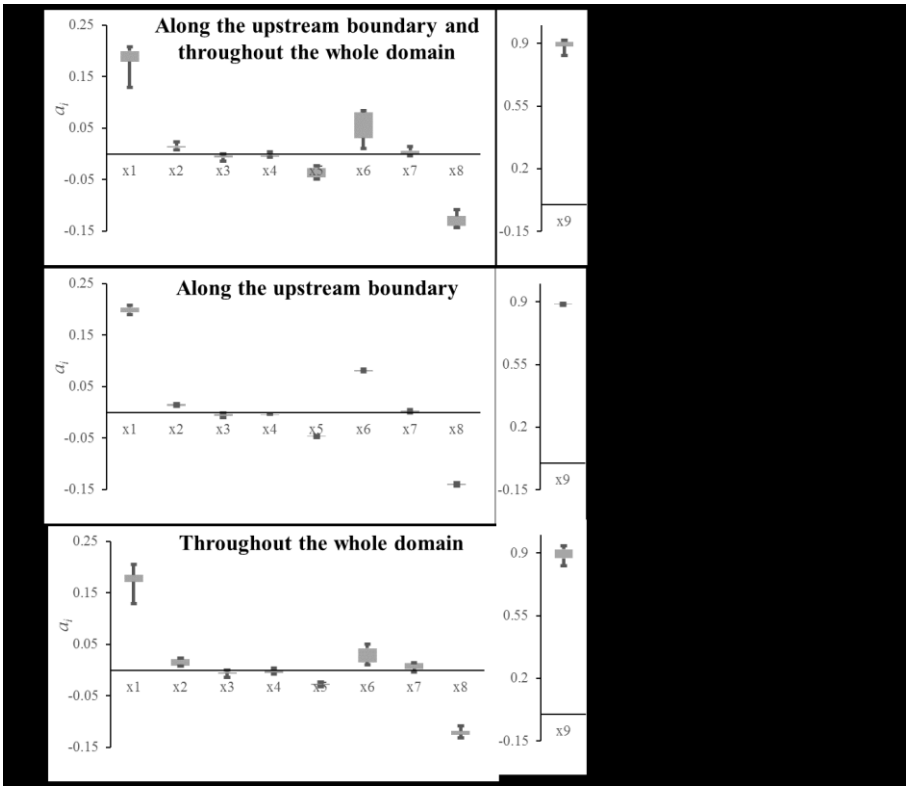

Figure 7: Sensitivity of the regression coefficients to choice of the indicator of flood severity by considering percentiles from 50th to 90th computed (a) either along the upstream boundaries of the domain, or throughout the whole domain and (b) along the upstream boundaries of the domain and (c) throughout the whole domain.

4.1.2. Sample size

We investigated whether the sample size (2,000 building layouts) is large enough to produce robust and reliable results. For this purpose, we selected randomly 1,500, 1,000, 500 and 250 configurations out of the initial sample. For each sub-sample, the random selection was performed 10,000 times to assess the sensitivity of the results to the selected configurations.

Like in Figure 7, we display the results in the form of boxplots obtained from the sets of regression coefficients corresponding to the 10,000 different sub-samplings (Figure 8). Again, the findings of section 3.3 are hardly affected by a reduction of the sample size, at least when the

subsample size remains above 1,000 (Figure 8). In all cases, the most influencing urban characteristic remains the building coverage (x_9) and only variables x_1, x_5, x_6, x_8 and x_9 show a significant influence on the computed water depths. Even for a sample size lower than 1,000, most of the results remain consistent with the findings of section 3.3, and only some coefficients show substantial variations. Hence, the sample size of 2,000 different building layouts is deemed sufficient.

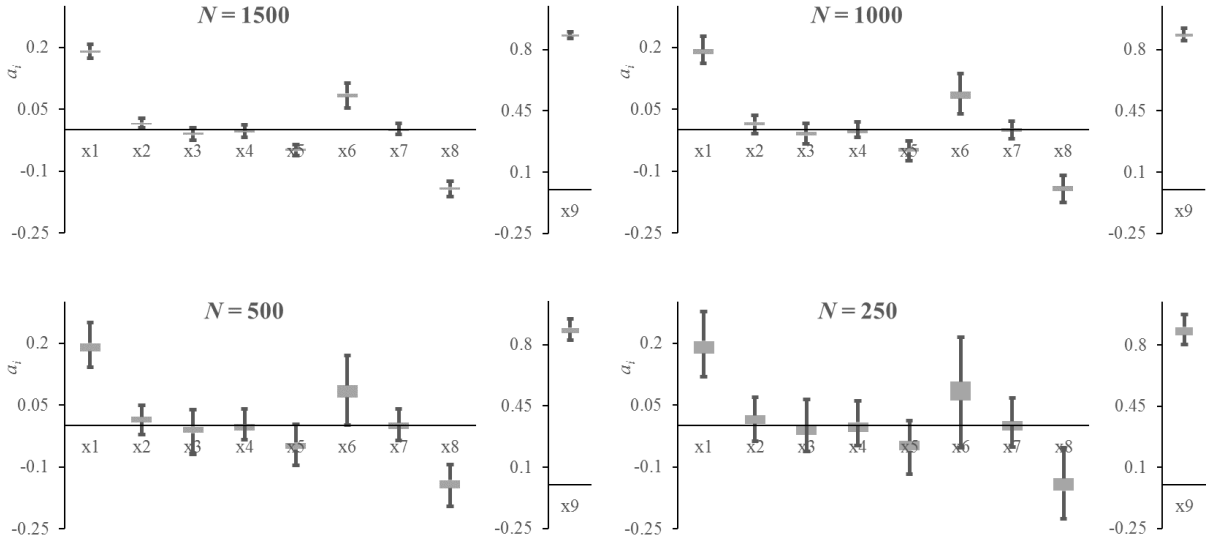

Figure 8: Sensitivity of the absolute values of the regression coefficients of the urban characteristics for Δh_{90} to the sample size (N).

4.1.3. Number of urban characteristics used in the regression analysis

The respective influence of each of the nine selected urban characteristics on the computed water depths was shown to be very different, suggesting that some of the urban characteristics could be neglected in the regression analysis. Here, we compare the predictive capacity of regressions based either on all urban characteristics (variables x_1 to x_9) or just on the most influential ones. The predictive capacity of each regression is assessed through the resulting root mean square error.

Using only the building coverage (x_9) for the linear regression leads to a root mean square error roughly 37% higher than with the MLR based on all variables (Table 4). The prediction of Δh_{90} based on the five most influential variables (x_1, x_5, x_6, x_8 and x_9) gives an accuracy similar to the one obtained with all nine variables.

Considered variables	x_9	x_1, x_5, x_6, x_8 and x_9	x_1 to x_9
Root mean square error (cm)	4.01	2.93	2.93

Table 4: Root mean square errors on the estimation of Δh_{90} for sets of urban characteristics used in the MLR.

4.1.4. Model choice

In all analyses above, a linear relationship was assumed between the rise in water depth $y = \Delta h_{90}$ and variables x_1 to x_9:

$$\overline{y} = a_0 + \sum_{i=1}^{9} a_i \overline{x}_i \qquad (6)$$

Here, we check whether our findings are affected by the choice of another model. For this purpose, we tested two approaches:

- First, we used an alternate model, assuming that Δh_{90} can be predicted by means of a power law involving all parameters x_1 to x_9:

$$\frac{y}{y_{\text{mean}}} = b_0 \prod_{i=1}^{9} \left(\frac{x_i}{x_{i,\text{mean}}} \right)^{b_i} , \qquad (7)$$

  in which b_0 to b_9 are coefficients to be calibrated. Coefficients b_i certainly do not take the same values as parameters a_i; but still their relative values provide an indication on which of the variables x_i have more influence on the determination of Δh_{90}.

- Second, we computed *Pearson correlation coefficients* ρ_i, which also reflect the link between variables, but it does so independently of the choice of a particular model.

In practice, the estimation of coefficients b_i in Eq. (7) is performed by means of a MLR, after applying a logarithmic transformation to variables x_i and y:

$$\ln\left(\frac{y}{y_{\text{mean}}}\right) = \ln b_0 + \sum_{i=1}^{9} b_i \ln\left(\frac{x_i}{x_{i,\text{mean}}}\right). \tag{8}$$

The configurations involving a street orientation (x_2) equal to zero were disregarded; but they represent only 2.5 % of all building layouts in the sample.

Coefficients a_i, b_i and ρ_i are compared in Figure 9. Each set of coefficients has been scaled so that the sum of the nine absolute values is one. The following observations can be made.

- In all three approaches, variables x_9 is shown to have a substantial influence on, or be strongly correlated with, the flood severity indicator Δh_{90}. The prevailing influence of the building coverage is therefore a robust outcome of the analysis.
- A difference between the different approaches is found for the mean parcel area (x_6). The Pearson correlation coefficients suggest that the importance of x_6 is similar to that of the building coverage (x_9), while has some influence in the standard MLR and multiple linear regression with logarithmic transform, but of a lower magnitude than that of x_9. This difference may result from the existing positive correlation between x_6 and x_9, as revealed in Figure 10. Given this correlation, the lower weight given to x_9 by the Pearson correlation compared to the standard MLR is simply compensated by a higher weight given to x_6.
- In all approaches, the coefficients assigned to the minor street width (x_5) and the building side setback (x_8) are consistently negative and of substantial magnitude. This confirms that considering variables x_5 and x_8 as strongly controlling the flow through the urban area is a robust outcome of the analysis.

- Similarly, the coefficients associated to the major street width x_4 (x_4) and the building rear setback (x_7) take consistently negative values of small magnitude, while those related to x_2 (street orientation) are also consistently small but positive. Therefore, these variables may safely be disregarded, as shown also in Table 4.
- The regression coefficients related to the average street length (x_1) and the street curvature (x_3) (a_1, a_3 and b_1, b_3) have an opposite sign compared to the corresponding Pearson correlation coefficients (ρ_1 and ρ_3). This is a result of the significant negative correlation between x_1 and x_3, as revealed in Figure 10. Although this correlation makes sense from an urban planning point of view, as a stronger street curvature implies more short streets in the inner area of the curved streets, it somehow hampers drawing truly robust conclusions on the relation between the street length and the upstream flood severity.
- Another interesting finding obtained from the Pearson regression coefficients is that several variables have a similar importance to x_9, while according to the standard MLR and the MLR with logarithmic transform, only x_9 seemed to be of prevailing influence. This result is consistent with those presented in the next section, which indicate that the building coverage is of lower importance than another composite indicator of flow *conveyance* at the scale of the urban area (district-scale), while x_9 is *stricto sensu* a proxy for the *storage* capacity (and not the conveyance capacity) in the urban area.

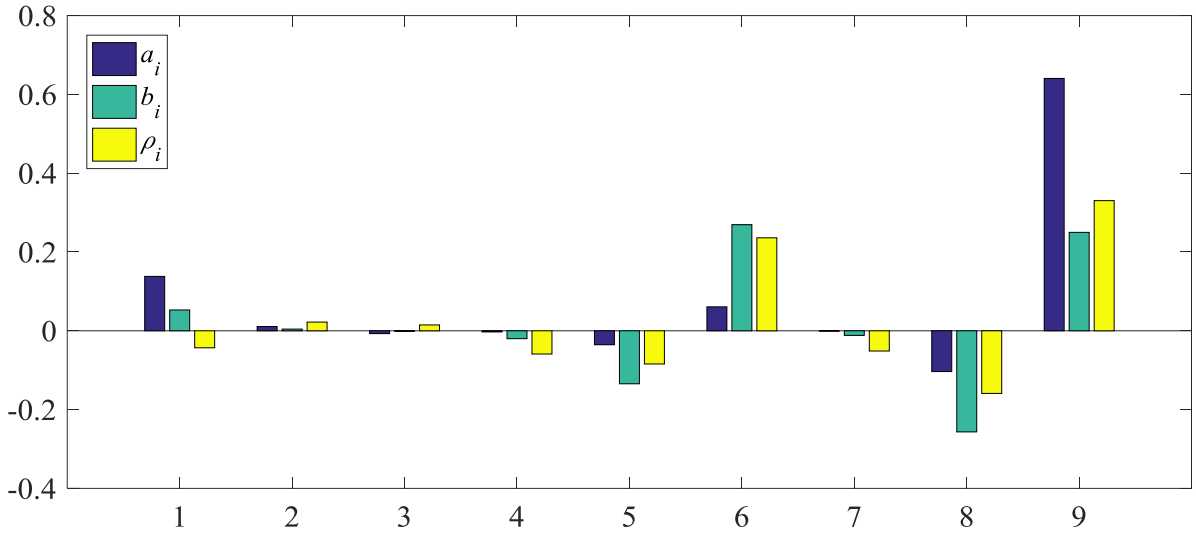

Figure 9: Comparison of regression coefficients a_i and b_i obtained from multiple linear regression, without and with logarithmic transform, and with Pearson correlation coefficients ρ_i. Each set of coefficients has been scaled so that the sum of the nine absolute values is one.

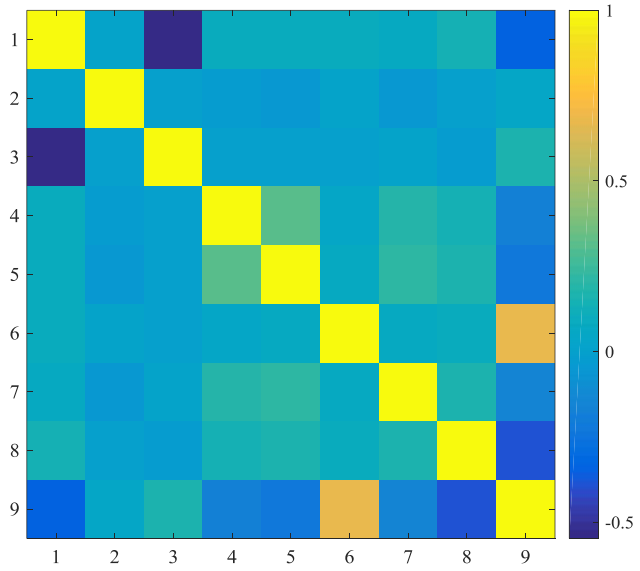

Figure 10: Pearson correlation coefficients between all variables x_1 to x_9.

4.2. Conceptual approach

The set of input variables x_1 … x_9 were selected for their significance in terms of urban planning. However, as such, they are neither optimal for statistical analysis (Figure 9) nor of direct relevance

for hydraulic analysis. Therefore, we present here a simple conceptual model, which relates these urban planning parameters to just two parameters of direct relevance for hydraulic analysis: a district-scale storage porosity Φ_D, and a district-scale conveyance porosity Ψ_D.

The district-scale storage porosity is straightforward to evaluate from the building coverage ($\Phi_D = 1 - x_9$), while the district-scale conveyance porosity was estimated based on an idealization of the geometry of the considered urban layouts. Despite a number of simplifying assumptions, we show that these two district-scale porosity parameters explain amazingly well the results obtained in section 3 for the whole set of 2,000 quasi-realistic urban configurations.

4.2.1. Conceptualization

First, we aim to derive an expression relating the district-scale conveyance porosity Ψ_D to the input parameters of relevance for urban planning, as listed in Table 1. To do so, we introduce the following simplifying assumptions, which enable obtaining analytical expression for Ψ_D (Figure 11):

- the street orientation and curvature are neglected ($\alpha = \chi = 0$), so that all streets are straight and aligned either along the west-east direction or the north-south direction;
- these streets are separated by building-blocks of identical size;
- the size of a building-block is given by the average street length L_s;
- all minor (resp. major) streets have the same width equal to w (resp. W);
- each building-block is split into several identical square parcels of length equal to the square root of the mean parcel area A_p;
- the size of a building is determined from the parcel area and the three setbacks s_f, s_r and s_s;

- we estimate the conveyance porosity as the minimum void fraction in a section normal to the west-east direction (as if the flow as aligned with this direction).

Consistently with the procedural modelling presented in section 2.1, the idealized building layouts considered here also comply with the following rules:

- one single major street is introduced in each direction;
- only the external parcels of the building-blocks are urbanized while the others remain undeveloped.

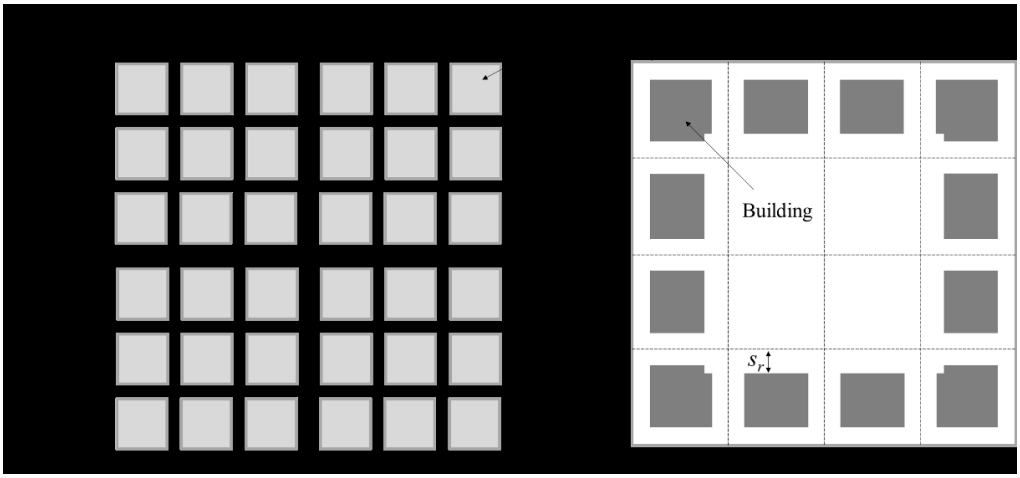

Figure 11: Idealized urban pattern at the district-scale (a) and block-scale (b).

Under these simplifying assumptions, the number n of building-blocks over the length L_D of the urban area can be derived from the urban parameters by:

$$L_D = (n-2)(L_s + w) + 2\left(L_s + \frac{w+W}{2}\right) \quad \Rightarrow \quad n = \frac{L_D - (W-w)}{L_s + w} \quad . \tag{9}$$

The number n_b of buildings (or parcels) over the length L_s of a building-block is simply equal to: $L_s / \sqrt{A_p}$.

The block-scale conveyance porosity Ψ_B is estimated as the ratio between the minimum free length along the north-south or east-west direction and the total length of the building-block L_s:

$$\Psi_B = \left(\frac{L_s}{\sqrt{A_p}} - 2 \right) \frac{2s_s}{L_s} + 2\frac{s_s + s_f}{L_s} \Rightarrow \Psi_B = 2\left(\frac{s_s}{\sqrt{A_p}} + \frac{s_f - s_s}{L_s} \right). \quad (10)$$

Similarly, the district-scale conveyance porosity Ψ_D is computed as:

$$\begin{aligned} \Psi_D &= (n-2)\frac{\Psi_b L_s + w}{L_D} + 2\frac{\Psi_b L_s + \frac{W+w}{2}}{L_D} \\ \Rightarrow \Psi_D &= \frac{\Psi_b L_s + w}{L_s + w} + \frac{w}{L_D}\left(\frac{W}{w} - 1 \right)\left(1 - \frac{\Psi_b L_s + w}{L_s + w} \right) \end{aligned} \quad (11)$$

4.2.2. Results

Based on the district-scale storage and conveyance porosities, Φ_D and Ψ_D, a regression analysis was performed using Eq. (12):

$$\Delta h_{90} = a\,(1-\Phi_D)^b\,(1-\Psi_D)^c \quad (12)$$

Since $\Delta h_{90} = 0$ for $\Phi_D = \Psi_D = 1$, Δh_{90} in Eq. (12) is logically expressed as a function of 1 - Φ_D and 1 - Ψ_D. The values of parameters *a*, *b* and *c* were determined by minimizing the root mean square error between Δh_{90} derived from Eq. (12) and the corresponding values extracted from the hydraulic simulations of the 2,000 building layouts (section 3.2.2).

Figure 12 shows the remarkable correlation obtained between Eq. (12), with calibrated coefficients $a = 1.63$, $b = 0.75$ and $c = 2.24$, and the reference values. The mean absolute and root mean square errors on the prediction of Δh_{90} from Eq. (12) over the 2,000 computed urban patterns are respectively equal to 2.0 cm and 2.6 cm.

Considering only the district-scale storage porosity in the regression analysis ($c = 0$) gives optimal coefficient $a = 1.00$ and exponent $b = 0.91$. The mean absolute and root mean square errors increase by respectively 47% and 57% when neglecting the district-scale conveyance

porosity in the regression analysis. Neglecting the district-scale storage porosity ($b = 0$), the errors increase dramatically by more than a factor 3.

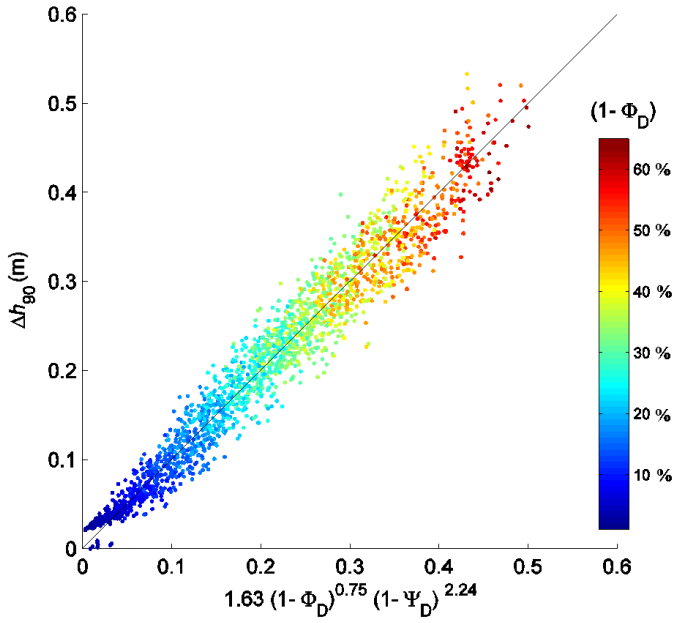

Figure 12: Relationships between the optimal regression analysis of the district-scale porosities Φ_D and Ψ_D and the inundation indicator Δh_{90} for the 2,000 computed urban patterns.

4.2.3. Interpretation

Although the conceptual model is based on an idealization of the building layouts and on relatively crude assumptions, the results obtained with this simple model are very promising. While the minimum value of the root mean square error computed with a regression analysis based on the nine urban characteristics is 2.9 cm (section 3.3), this error is found here to drop to 2.6 cm when only the two district-scale porosity parameters are used.

The standard MLR analysis indicates that the storage porosity (i.e. the building coverage) is by far the urban characteristic influencing most the water depths (section 3.3); but this is somehow misleading since we find here, based on parameters of direct hydraulically significance, that the conveyance porosity has actually an even stronger influence (exponent $c = 2.24$ ~ 3 × exponent b). This aspect was already suggested in section 4.1.4, which highlighted that other parameters than the building coverage (x_9) seem to have a similar importance when a

logarithmic transformation was applied to all variables, as well as based on Pearson regression coefficients.

However, the storage porosity is a key parameter to capture the influence of urban patterns on inundation water depths. While the accuracy of the conceptual model decreases by around 50% when neglecting the conveyance porosity, it drops by a factor 3 when the storage porosity is not considered.

4.2.4. Implication for urban planning

Figure 13 provides two examples of pairs of building layouts leading to similar water depths upstream, although they are characterized by significantly different building coverage ratios, i.e. different values of the district-scale storage porosity ($\Phi_D \sim 0.6$ vs. $\Phi_D \sim 0.8$). In both cases, the higher value of the building coverage is compensated by a higher value of the district-scale conveyance porosity.

These results are fully consistent with Eq. (12), which highlights that potential detrimental effect of reduction of the storage porosity (i.e. new developments increasing the building coverage) can be mitigated by means of a suitable layout of the buildings which increases the conveyance porosity. This finding is of high relevance to guide more flood-resilient urban developments.

Eqs (10) and (11) reveal that the district-scale conveyance porosity can be increased mainly in two ways:

- at the district-scale, increasing the fragmentation of the urban pattern (i.e. increasing the value of n) by reducing the average street length L_s or by favouring a high number of narrow streets to a low number of large ones;
- at the building-block-scale, increasing the building side setback s_s or reducing the building size (i.e. reducing the mean parcel area $\sqrt{A_p}$).

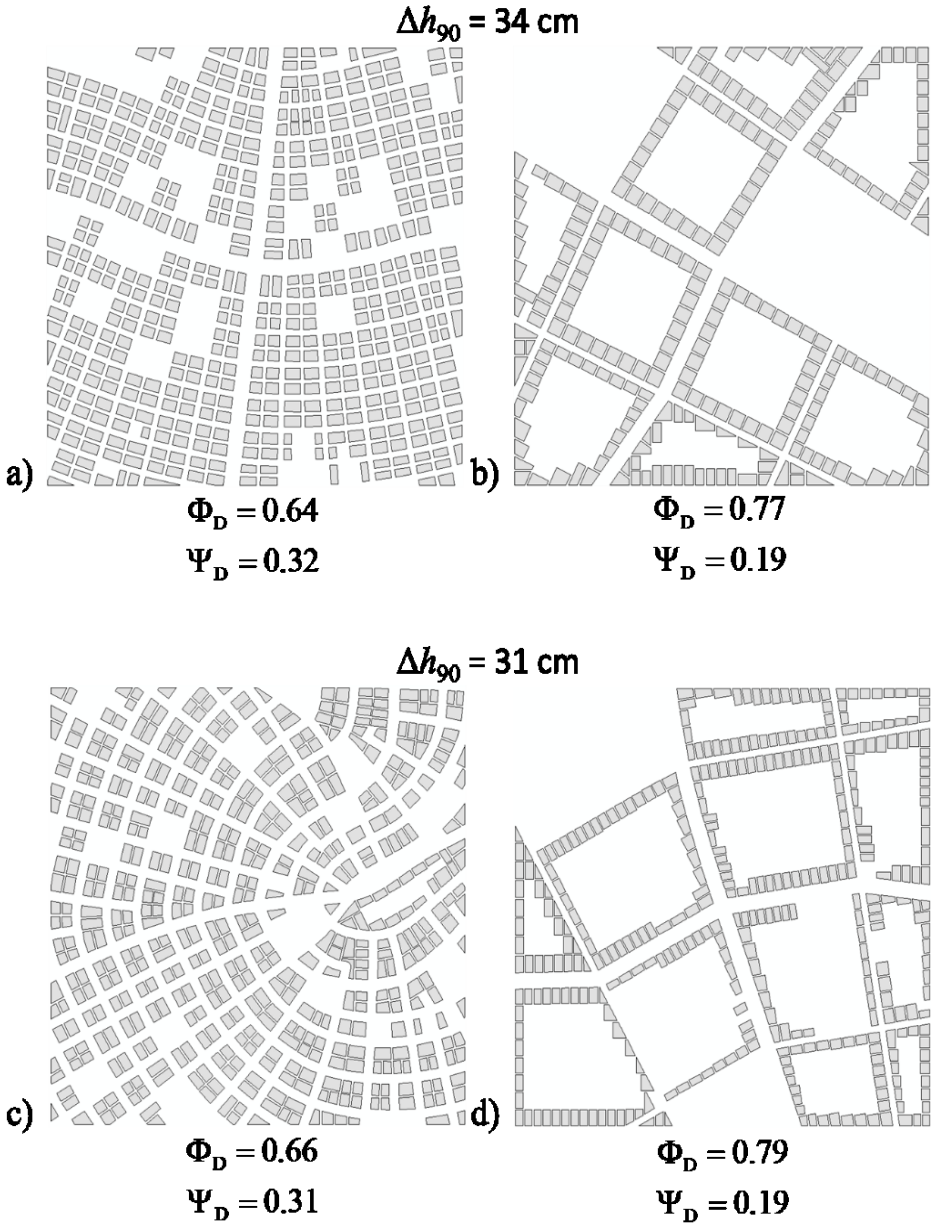

Figure 13 : Urban patterns with different district-scale porosity values leading to similar upstream water depths.

The findings described above were obtained based on fixed hydraulic boundary conditions. Nonetheless, the overall conclusions would certainly remain unchanged if, for instance, the inflow magnitude was varied. Indeed, we expect that increasing (resp. decreasing) the inflow discharge would mainly magnify (resp. shrink) the water level differences between the upstream and downstream faces of the urban area for all configurations, without changing substantially the

flow distribution within the street network. This effect was shown by Arrault et al. (2016) based on a laboratory model of an urban district, in which the inflow discharge was varied systematically over one order of magnitude (see Figure S1 in Supplement to Arrault et al. 2016). Consequently, varying the inflow discharge is unlikely to substantially modify the ranking of the various building layouts in terms of flood-resilience. Similarly, Arrault et al. (2016) demonstrated that varying the inflow partition between the upstream faces has a limited influence on the flow within the urban area. In contrast, introducing a bottom slope would promote higher flow velocity so that parameters which play a little part in the configuration considered here (flat bottom) would become far more important (e.g., street orientation and curvature, as mentioned in Section 3.3).

5. CONCLUSION

This paper presents a unique systematic study of inundation flow in quasi-realistic urbanized areas, which links hydraulic modelling results to parameters of direct significance for urban planning. Based on porosity-based hydraulic computations of inundation flow for a set of 2,000 different building layouts, the relative influence of nine urban characteristics (average street length, street orientation and curvature, major and minor street widths, mean parcel area, rear and side building setbacks and building coverage) on inundation water depths were assessed. We focused on the water depth upstream of the considered urban area, as it reflects the impact of the developed area on the severity of flooding upstream. The terrain slope was neglected, so that the analysis results apply mostly to floodplains of typical lowland rivers.

The most influential parameters were found to be the building coverage, the mean parcel area (controlling directly the building size), the building side-setbacks, and to a lesser extent, the length and width of the streets. For the tested configurations, the more fragmented the urban pattern is (relatively small parcel sizes and street length), the lower the upstream water depths. This aspect is related to urban design at the district and building-block scales. Additionally,

increasing the voids in-between the buildings (i.e. larger side setbacks) was shown to also contribute to a decrease in the upstream waterdepth. This aspect relates to urban planning at the local level of a single parcel.

We also built a simple conceptual model based on storage and conveyance porosity parameters determined at the district-scale. Although particularly simple, the model was shown to provide surprisingly accurate predictions of the influence of the building layout on upstream water depths. The model parameters reveal that an increase in building coverage in an urban area (i.e. new developments, leading to a decrease in the district-scale storage porosity) can be compensated by a suitable location of the buildings so that the district-scale conveyance capacity increases.

This study paves the way for more quantitative approaches in water-sensitive urban design, based on process-oriented modelling of the interactions between complex urban systems and flooding mechanisms, enabling more flood-resilient urban developments.

Further research is needed to reach a deeper understanding of the influence of environmental parameters, such as the terrain slope and imperviousness, man-made structures (sewage system, underground structures …) and obstacles (cars, trees …) as well as varying hydraulic conditions (unsteady flood waves, pluvial flooding …).

ACKNOWLEDGEMENTS

The research was funded through the ARC grant for Concerted Research Actions, financed by the Wallonia-Brussels Federation.

REFERENCES

Arrault, A., P. Finaud-Guyot, P. Archambeau, M. Bruwier, S. Erpicum, M. Pirotton, and B. Dewals. 2016. Hydrodynamics of long-duration urban floods: Experiments and numerical modelling. Natural Hazards and Earth System Sciences 16:1413–1429.

Bazin, P.-H. 2013. Flows during floods in urban areas : influence of the detailed topography and exchanges with the sewer system. . Université Claude Bernard - Lyon I.

Beckers, A., B. Dewals, S. Erpicum, S. Dujardin, S. Detrembleur, J. Teller, M. Pirotton, and P. Archambeau. 2013. Contribution of land use changes to future flood damage along the river Meuse in the Walloon region. Natural Hazards and Earth System Sciences 13:2301–2318.

Bruwier, M., P. Archambeau, S. Erpicum, M. Pirotton, and B. Dewals. 2017a. Shallow-water models with anisotropic porosity and merging for flood modelling on Cartesian grids. Journal of Hydrology 554:693–709.

Bruwier, M., S. Erpicum, P. Archambeau, M. Pirotton, and B. Dewals. 2017b. Discussion of "Computing flooding of crossroads with obstacles using a 2D numerical model" by P.-H. Bazin, E. Mignot and A. Paquier. Journal of Hydraulic Research.

Bruwier, M., S. Erpicum, M. Pirotton, P. Archambeau, and B. J. Dewals. 2015. Assessing the operation rules of a reservoir system based on a detailed modelling chain. Natural Hazards and Earth System Sciences 15:365–379.

Chen, A. S., B. Evans, S. Djordjević, and D. A. Savić. 2012. A coarse-grid approach to representing building blockage effects in 2D urban flood modelling. Journal of Hydrology 426–427:1–16.

de Wit, M. J. M., H. A. Peeters, P. H. Gastaud, P. Dewil, K. Maeghe, and J. Baumgart. 2007. Floods in the Meuse basin: Event descriptions and an international view on ongoing measures. International Journal of River Basin Management 5:279–292.

Detrembleur, S., F. Stilmant, B. Dewals, S. Erpicum, P. Archambeau, and M. Pirotton. 2015. Impacts of climate change on future flood damage on the river Meuse, with a distributed uncertainty analysis. Natural Hazards 77:1533–1549.

Dottori, F., G. Di Baldassarre, and E. Todini. 2013. Detailed data is welcome, but with a pinch of salt: Accuracy, precision, and uncertainty in flood inundation modeling. Water Resources Research 49:6079–6085.

El Kadi Abderrezzak, K., A. Paquier, and E. Mignot. 2009. Modelling flash flood propagation in urban areas using a two-dimensional numerical model. Natural Hazards 50:433–460.

Ernst, J., B. J. Dewals, S. Detrembleur, P. Archambeau, S. Erpicum, and M. Pirotton. 2010. Micro-scale flood risk analysis based on detailed 2D hydraulic modelling and high resolution geographic data. Natural Hazards 55:181–209.

Erpicum, S., B. Dewals, P. Archambeau, and M. Pirotton. 2010. Dam-break flow computation based on an efficient flux-vector splitting. Journal of Computational and Applied Mathematics 234:2143–2151.

Ghostine, R., I. Hoteit, J. Vazquez, A. Terfous, A. Ghenaim, and R. Mose. 2015. Comparison between a coupled 1D-2D model and a fully 2D model for supercritical flow simulation in crossroads. Journal of Hydraulic Research 53:274–281.

Huang, C.-J., M.-H. Hsu, W.-H. Teng, and Y.-H. Wang. 2014. The impact of building coverage in the metropolitan area on the flow calculation. Water (Switzerland) 6:2449–2466.

Kim, B., B. F. Sanders, J. S. Famiglietti, and V. Guinot. 2015. Urban flood modeling with porous shallow-water equations: A case study of model errors in the presence of anisotropic porosity. Journal of Hydrology 523:680–692.

Kim, B., B. F. Sanders, J. E. Schubert, and J. S. Famiglietti. 2014. Mesh type tradeoffs in 2D hydrodynamic modeling of flooding with a Godunov-based flow solver. Advances in Water Resources 68:42–61.

Lin, E., K. Shaad, and C. Girot. 2016. Developing river rehabilitation scenarios by integrating landscape and hydrodynamic modeling for the Ciliwung River in Jakarta, Indonesia. Sustainable Cities and Society 20:180–198.

Mignot, E., A. Paquier, and S. Haider. 2006. Modeling floods in a dense urban area using 2D shallow water equations. Journal of Hydrology 327:186–199.

Özgen, I., D. Liang, and R. Hinkelmann. 2016a. Shallow water equations with depth-dependent anisotropic porosity for subgrid-scale topography. Applied Mathematical Modelling 40:7447–7473.

Özgen, I., J. Zhao, D. Liang, and R. Hinkelmann. 2016b. Urban flood modeling using shallow water equations with depth-dependent anisotropic porosity. Journal of Hydrology 541:1165–1184.

Parish, Y. I. H., and P. Müller. 2001. Procedural modeling of cities. Proceedings of the 28th Annual Conference on Computer Graphics and Interactive Techniques,:301–308.

Prusinkiewicz, P., and A. Lindenmayer. 1990. Modeling of cellular layers. The Algorithmic Beauty of Plants:145–174.

Sanders, B. F., J. E. Schubert, and H. A. Gallegos. 2008. Integral formulation of shallow-water equations with anisotropic porosity for urban flood modeling. Journal of Hydrology 362:19–38.

Schubert, J. E., and B. F. Sanders. 2012. Building treatments for urban flood inundation models and implications for predictive skill and modeling efficiency. Advances in Water Resources 41:49–64.

Vanegas, C. A., D. G. Aliaga, B. Beneř, and P. A. Waddell. 2009. Interactive design of urban spaces using geometrical and behavioral modeling. ACM Transactions on Graphics 28:111:1–111:9.

Vollmer, D., D. Costa, E. S. Lin, Y. Ninsalam, K. Shaad, M. F. Prescott, S. Gurusamy, F. Remondi, R. Padawangi, P. Burlando, C. Girot, A. Grêt-Regamey, and J. Rekittke. 2015. Changing the Course of Rivers in an Asian City: Linking Landscapes to Human Benefits through Iterative Modeling and Design. Journal of the American Water Resources Association 51:672–688.